ISSN 2706-655X Vol.6, Issue 4: 31-38, DOI: 10.25236/IJFET.2024.060406

Numerical investigation of flow and heat transfer characteristics in a fluidized bed solar particle receiver

Peng Wang*, Yonghua Li

School of Energy, Power and Mechanical Engineering, North China Electric Power University, Baoding, 071003, China
**Corresponding author: liverpooler@foxmail.com*

Abstract: *The fluidized bed solar particle receiver (SPR) has the potential to be used widely in the next generation concentrated solar power (CSP) plant as its high operating temperature, excellent stability and high energy storage capacity. However, the particle circulation pattern and temperature distribution are difficult to be visualized and measured by experimental methods, and there is a lack of improvement on the internal structure of the receiver. In this contribution, a three-dimensional transient numerical model is developed to study the flow and heat transfer characteristics under solar radiation. The solid particles show a clear symmetrical distribution in the receiver at the initial moment. With the continuous access of the gas, the movement of particles in the receiver becomes random and irregular. The average particle temperature can reaching 1645.34 K after 10 s, but the temperature rise rate of the particles gradually weakens. In the radial direction, the radiation distribution shows a likely Gaussian distribution. Simulation results can provide reference for the design and improvement of solar particle receiver. The radiation intensity gradually increases with the increase of axial height, and finally remains stable.*

Keywords: *Solar particle receiver, heat transfer, multiphase flow, structure improvement*

1. Introduction

Concentrated solar power (CSP) plays a crucial role in developing low-carbon economy and meeting the global energy consumption[1]. One of the major advantages of the CSP technologies over other renewable energy technologies is the ability to integrate with large-scale thermal energy storage (TES) systems and subsystems easily, which allows them to resist fluctuations in solar irradiation and to provide continuous and stable power outputs for large-scale solar grid-connected power generation system[2]. The central receiver is the essential part of a CSP plant, which absorbs the concentrated solar radiation directly by heat transfer medium (HTM). Compared to other conventional HTMs, such as molten salts, solid particles have more advantages, including stable chemical property, low cost, high operating temperature and so on[3,4]. Therefore, solar particle receiver (SPR) is considered as the most promising technology for the next generation CSP plant, which is increasingly popular, gaining more attention from scholars and researchers.

The concept of SPR was firstly proposed by Hruby et al.[5,6] in 1980s. Since then, there have been two main research methods to investigate the SPR. One is experimental methods, the other is numerical simulation. Many parameters can be measured by experimental methods, such as particle temperature, gas velocity, particle residence time. Rightley et al.[7] measured radiative heat flux and particle temperatures in a free-falling SPR. In 2008, Siegel et al.[8] firstly conducted experimental test under real solar irradiation. The results demonstrated that the particle temperature increased 250 K most and the thermal efficiency could exceed 50%. Ho et al.[9] carried out experiments to study the heat transfer and flow characteristics of a free-falling receiver. They noticed that the thermal efficiency of the receiver increased as the particle mass flow rate rose.

Nevertheless, it is difficult to obtain precise flow and heat transfer characteristics at acceptable cost by experiment. These years, with the development of computer science and numerical algorithms, numerical simulation is increasingly popular. Scholars has designed SPRs with a variety of geometry structures. For example, Tan et al.[10] built a three-dimensional numerical model and investigated how the particle diameter affected the performance of the free-falling receiver. They found that the particle with smaller diameter has higher outlet particle temperature. A numerical simulation to investigate the

ISSN 2706-655X Vol.6, Issue 4: 31-38, DOI: 10.25236/IJFET.2024.060406

effect of recirculating flow and vortex flow on the SPR was conducted by Sarker et al.[11,12]. They concluded that the thermal efficiency of recirculating flow SPR was around 30% higher which of vortex flow SPR. Wu et al.[13–15] developed a new kind of centrifugal SPR. When the input irradiation was 670 kW m^{-2}, the the outlet particle temperature could reach 900 ℃ and the thermal efficiency was between 71% and 79%. Recently, Xiao et al.[16,17] devised a spiral SPR. They found that the temperature of particle exceeded 625 ℃ when the particle mass flow rate was 0.21 kg s^{-1}.

Although there are many studies about solar particle receiver using numerical method, there have been few reports about the circulation behavior of the system and the distribution of solid motion and temperature. Thus, in this study, we develop a numerical model to investigate the flow and heat transfer characteristics of a rectangular tube fluidized bed SPR, which would provide significant guidance for the design and optimization of solar particle receiver.

2. Model descriptions

2.1 Physical model

A typical fluidized bed SPR consists of several parallel tubes. To simplify the simulation, we take one tube for analysis. The structural design of the single tube receiver is shown in Fig.1. The depth of the receiver is designed as 6.4 mm due to the need to prevent significant particle temperature differences between the side exposed to solar irradiation and the side facing the back wall. Solid particles are initially stored at the bottom of the receiver. Firstly, solid particles receive solar irradiation fed through the tube wall and move intensely in the receiver as the gas flows into the receiver. Subsequently, the heated particles exchange energy with the cold gas. Finally, heated gas flows out from the outlet after the heat transfer process.

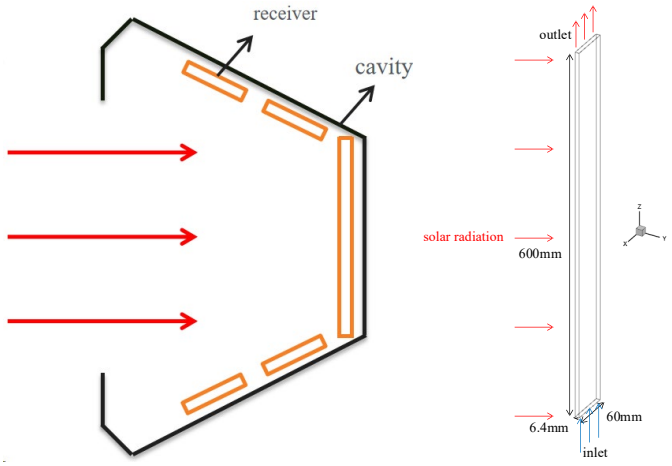

Figure 1: Schematic of the fluidized bed SPR.

2.2 Governing equations for gas phase

The model notation used in this article is as follows:

1)Nomenclature

symbol	implication	symbol	implication
t	time, s	s	direction
u	velocity, m s^{-1}	Re	Reynolds number
p	pressure, Pa	A	area surface, m^2
g	acceleration of gravity, m s^{-2}	k	thermal conductivity, W m^{-1} K^{-1}
C_D	drag coefficient	Nu	Nusselt number
d	diameter, m	Pr	Prandtl number
C_p	specific heat capacity, J kg^{-1} K^{-1}	$\overline{\overline{I}}$	unit vector
T	temperature, K	h	Heat transfer coefficient, W m^{-2} K^{-1}
m	mass, kg	I	Radiation intensity, W m^{-2}
S	source term	a	absorption coefficient
r	position	n	refraction coefficient,

ISSN 2706-655X Vol.6, Issue 4: 31-38, DOI: 10.25236/IJFET.2024.060406

2)Greek symbols

symbol	implication	symbol	implication
α	volume fraction	$\overline{\overline{\tau}}$	stress-strain tensor
ρ	density, kg m^{-3}	σ_s	scattering coefficient
λ	bulk viscosity, N s m^{-2}	σ	Stefan-Boltzmann constant
μ	dynamic viscosity, N s m^{-2}	φ	phase function
β	momentum exchange coefficient	Ω'	three-dimensional space angle

3) Subscripts

symbol	implication
f	gas fluid phase
p	solid particle phase

Gas phase in the fluidized bed SPR is regarded as the continuous fluid medium and solved by the Navier-Stokes equations. The mass, momentum, and energy conservation equations for gas phase can be written as

$$\frac{\partial}{\partial t}\left(\alpha_f \rho_f\right)+\nabla\cdot\left(\alpha_f \rho_f \vec{u}_f\right)=0 \tag{1}$$

$$\frac{\partial}{\partial t}\left(\alpha_f \rho_f \vec{u}_f \vec{u}_f\right)+\nabla\cdot\left(\alpha_f \rho_f \vec{u}_f \vec{u}_f\right)=-\alpha_f \nabla p+\nabla\cdot\left(\alpha_f \overline{\overline{\tau}}_f\right)+\alpha_f \rho_f \vec{g}-\beta\left(\vec{u}_f-\vec{u}_p\right) \tag{2}$$

$$\frac{\partial}{\partial t}\left(\alpha_f \rho_f C_{p,f} T_f\right)+\nabla\cdot\left(\alpha_f \rho_f \vec{u}_f C_{p,f} T_f\right)=\nabla\cdot\left(\alpha_f k_{f,eff}\nabla T_f\right)-h\left(T_f-T_p\right) \tag{3}$$

where α_f, ρ_f, $\vec{u}_f$, $C_{p,f}$, T_f and $k_{f,eff}$ are the volume fraction, density, velocity, specific heat capacity, temperature and effective thermal conductivity of the gas phase respectively. p and $\vec{g}$ are the pressure and gravity acceleration. $\vec{u}_p$ is the velocity of the particle phase. $\overline{\overline{\tau}}_f$ involves the stress-strain tensor of the gas phase, and the equation is as follows

$$\overline{\overline{\tau}}_f=\alpha_f \mu_f\left(\nabla\vec{u}_f+\nabla\vec{u}_f^{\,T}\right)+\alpha_f\left(\lambda_f-\frac{2}{3}\mu_f\right)\nabla\cdot\vec{u}_f\,\overline{\overline{I}} \tag{4}$$

where μ_f, λ_f represent the dynamic and bulk viscosity of the gas phase. $\overline{\overline{I}}$ is the unit vector. β represents the the momentum exchange coefficient of fluid phase and particle phase. It enables to be calculated by the equation proposed by Ergun[18]

$$\beta=\begin{cases}150\dfrac{\left(1-\alpha_f\right)^2\mu_f}{\alpha_f d_p^2}+1.75\left(1-\alpha_f\right)\dfrac{\rho_f}{d_p}\left|\vec{u}_f-\vec{u}_p\right| & \text{if } \alpha_f<0.8\\ \dfrac{3}{4}C_D\dfrac{\left(1-\alpha_f\right)\alpha_f}{d_p}\rho_f\left|\vec{u}_f-\vec{u}_p\right|\alpha_f^{-2.65} & \text{if } \alpha_f>0.8\end{cases} \tag{5}$$

where d_p is the diameter of solid particles. C_D represents the drag coefficient, where the equation is

$$C_D=\begin{cases}24/Re\left(1+0.15Re^{0.687}\right) & Re<1000\\ 0.44 & Re\geq 1000\end{cases} \tag{6}$$

where Re is computed by

ISSN 2706-655X Vol.6, Issue 4: 31-38, DOI: 10.25236/IJFET.2024.060406

$$Re = \frac{\rho_f \alpha_f \left| \vec{u}_f - \vec{u}_p \right| d_p}{\mu_f} \tag{7}$$

where h is heat transfer coefficient, being computed by the following correlation:

$$Nu = \begin{cases} 2 + 0.6\varphi_f^{3.5} Re^{1/2} Pr^{1/3}, \mathrm{Re} < 200 \\ 2 + 0.5\varphi_f^{3.5} Re^{1/2} Pr^{1/3} + 0.02\varphi_f^{3.5} Re^{0.8} Pr^{1/3}, 200 < \mathrm{Re} < 1500 \\ 2 + 0.000045\varphi_f^{3.5} Re^{1.8}, \mathrm{Re} > 1500 \end{cases} \tag{8}$$

$$h = \frac{Nuk_f}{d_p} \tag{9}$$

2.3 Governing equations for solid particle phase

In the model of solid particle phase, we adopt the Euler-Euler model to investigate the solid motion and energy transfer. Solid particle is regarded as the continuous fluid. The governing equations for particle phase are written as

$$\frac{\partial}{\partial t}\left(\alpha_p \rho_p\right) + \nabla \cdot \left(\alpha_p \rho_p \vec{u}_p\right) = 0 \tag{10}$$

$$\frac{\partial}{\partial t}\left(\alpha_p \rho_p \vec{u}_p \vec{u}_p\right) + \nabla \cdot \left(\alpha_p \rho_p \vec{u}_p \vec{u}_p\right) = -\alpha_p \nabla p - \nabla p_p + \nabla \cdot \left(\alpha_p \overline{\overline{\tau}}_p\right) + \alpha_p \rho_p \vec{g} + \beta\left(\vec{u}_f - \vec{u}_p\right) \tag{11}$$

$$\frac{\partial}{\partial t}\left(\alpha_p \rho_p C_{p,p} T_p\right) + \nabla \cdot \left(\alpha_p \rho_p \vec{u}_p C_{p,p} T_p\right) = \nabla \cdot \left(\alpha_p k_{p,eff} \nabla T_p\right) + h\left(T_f - T_p\right) + S_{p,rad} \tag{12}$$

where α_p, ρ_p, $\vec{u}_p$, $C_{p,p}$, T_p and kf,eff are the volume fraction, density, velocity, specific heat capacity, temperature and effective thermal conductivity of the solid particle phase respectively. pp is the particle pressure. Sp,rad is the radiation source term for particle absorption. $\overline{\overline{\tau}}_p$ involves the stress-strain tensor of the particle phase, and the equation is as follows

$$\overline{\overline{\tau}}_p = \alpha_p \mu_p \left(\nabla \vec{u}_p + \nabla \vec{u}_p^{\,T}\right) + \alpha_p \left(\lambda_p - \frac{2}{3}\mu_p\right) \nabla \cdot \vec{u}_p \overline{\overline{I}} \tag{13}$$

where μ_p, λ_p represent the dynamic and bulk viscosity of the gas phase.

2.4 Radiation model

The DO radiation model is selected to load the solar radiation. Compared with other radiation models such as P1 model and Rosseland model, the advantage of the DO radiation model is that it can deal with the radiation in the semi-transparent medium. The fluidized bed solar particle receiver generally uses quartz glass as the material for manufacturing the receiver, which is the semi-transparent medium, so it is suitable for the DO radiation model. The radiation transport equation in the $\vec{s}$ direction at position $\vec{r}$ is:

$$\frac{dI\left(\vec{r}, \vec{s}\right)}{ds} + \left(a + \sigma_s\right) I\left(\vec{r}, \vec{s}\right) = an^2 \frac{\sigma T^4}{\pi} + \frac{\sigma_s}{4\pi} \int_0^{4\pi} I\left(\vec{r}, \vec{s}\right) \varphi\left(\vec{s}, \vec{s}'\right) d\Omega' \tag{14}$$

ISSN 2706-655X Vol.6, Issue 4: 31-38, DOI: 10.25236/IJFET.2024.060406

where I, a, s, n, σ_s are the radiation intensity, absorption coefficient, path length, refraction coefficient, scattering coefficient. σ is the Stefan-Boltzmann constant. T is the temperature of the location. φ is the phase function. Ω, is the three-dimensional space angle.

2.5 Boundary conditions

Fig.1 illustrates the computational domain of the fluidized bed SPR. In this study, the geometry is a rectangular tube with size of 60 mm (x direction)×6.4 mm (y)×600 mm (z). A non-slip boundary condition is assigned to the four side walls. The velocity inlet boundary condition is used to the inlet, while the pressure outlet boundary condition is applied to the outlet. A constant solar radiation is added to the wall on one side of the receiver, and the temperature of the wall is calculated according to the radiation intensity. The remaining walls are set as non-slip boundary condition.

2.6 Numerical methodology

Commercial software Ansys/Fluent 2020 R2 is employed for the calculations and simulations of the fluid phase. The RNG k-ε turbulence model with the standard wall function is used to model the transient state turbulent flow field. We utilize the Phase Coupled SIMPLE algorithm to couple the momentum and pressure. The equations for void fraction, momentum and energy are discretized by the First Order Upwind scheme. A uniform hexahedral grid is used to the discretize the computational domain, which is shown in Fig.2. We divide the receiver into 20(x direction)×8(y)×200(z) elements. The grid independence test is conducted. The results shows that the biggest relative error of the gas outlet temperature is less than 1%, which indicates that the grid we use meet the requirement of grid independence.

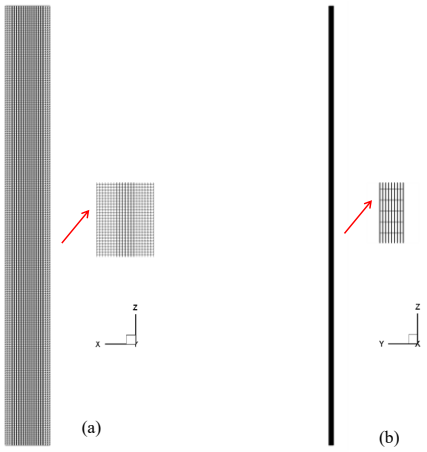

Figure 2: The schematic diagram of the grid (a) x-z plane (y=0 m) (b) y-z plane (x=0 m).

2.7 Operating conditions

The physical properties of the particles and gas are shown in Table 1. The solid particles are accumulated at a height of 0.05 m at the bottom of the fluidized bed receiver, and the volume fraction is 50 %. The airflow velocity is 3m·s^{-1}, the initial temperature of the gas phase is 300 K. The gas flows into the receiver, after experiencing sufficient convective heat transfer with solid particles, then flows out from the top outlet of the receiver. Simulations are conducted in real time for 10 seconds.

Table 1: Properties of gas and particle.

Properties	Gas	Particles
Density (kg m^{-3})	1.225	2490
Specific heat(J kg^{-1} K^{-1})	1006.43	840
Thermal conductivity(W m^{-1} K^{-1})	0.0242	1.1
Viscosity(kg m^{-1} s^{-1})	1.7894×10^{-5}	-
Diameter(mm)	-	0.8
Absorption coefficient	-	0.9
Scattering coefficient	-	0.1

ISSN 2706-655X Vol.6, Issue 4: 31-38, DOI: 10.25236/IJFET.2024.060406

2.8 Model validation

Simulations results have been validated by comparing them with numerical and experimental results of Patil et al. They carried out a series of fluidization experiments utilizing visual/infrared imaging technique. In their experiments, a container was filled with high-temperature particles and then fed with a constant stream of nitrogen at 293.15 K through a perforated plate at the bottom. Fig.3 shows the comparison between the numerical results and experimental data of the model developed in this paper for the same operating condition. It is evident that the predicted results of particle mean temperature agree with the previous experimental data, which verifies the numerical model we propose is trustworthy.

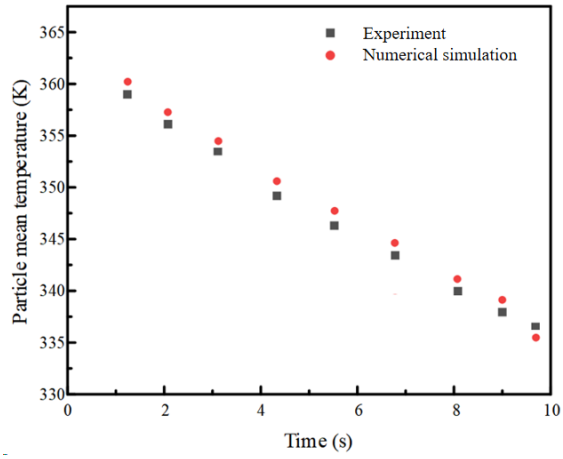

Figure 3: Comparison between the simulation results and the experimental data

3. Results and discussions

3.1 Particle volume fraction and velocity distribution

As the core component of the CSP system, it is necessary to investigate the flow and heat transfer characteristics of the fluidized bed solar particle receiver. Fig.4 shows the transient volume fraction distribution of solid particles in the central section of the fluidized bed receiver. It can be seen from Fig.4 that after the airflow enters the receiver from the bottom inlet, the solid particles move upward under the traction of the airflow and move in the height range of 0.1 m-0.2 m. Subsequently, due to the effect of gravity, the solid particles gradually fall from the region near the walls on both sides. In the first 1 s, the solid particles inside the receiver show a clear symmetrical distribution.

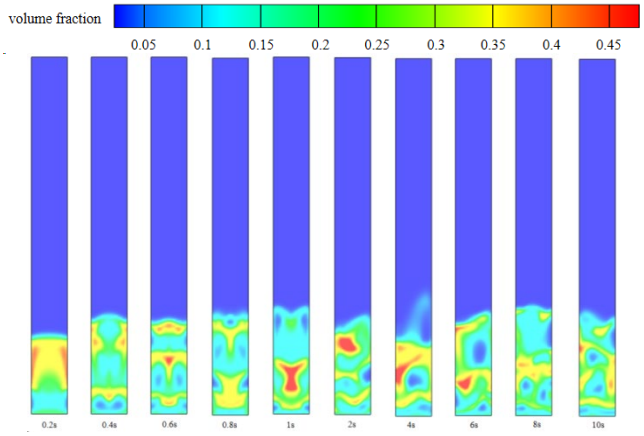

Figure 4: Transient distribution of solid particle in center section.

Fig.5 is the radial velocity distribution of solid particle at different axial heights in the central section of the fluidized bed receiver. It can be seen from Fig.5 that at the bottom area of the bed, which is the axial height of 0.01 m, the radial velocity of the solid particles is centrally symmetrical, which means that the solid particles move to the central area of the fluidized bed. In the upper part of the bed, which is the axial height of 0.15 m, the radial velocity of the solid particles is also symmetrically distributed,

ISSN 2706-655X Vol.6, Issue 4: 31-38, DOI: 10.25236/IJFET.2024.060406

but the direction is opposite, which means that the solid particles move to both sides of the wall. At the bottom region, the solid particles move radially to the central region of the fluidized bed due to the entrainment of bubbles. At the top of the bed, due to the rupture of the bubble, the solid particles are sprayed out to both sides and move radially to both sides of the wall, which is opposite to the movement direction of the particles at the bottom.

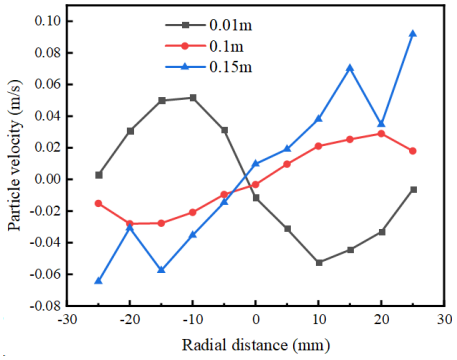

Figure 5: The radial velocity distribution of solid particles at different axial heights in the central section.

3.2 Particle temperature and radiation distribution

During actual operation process, the fluidized bed involves changes in gas-solid temperature and the exchange of energy between two different phases. Therefore, the gas-solid heat transfer characteristics have great significance to the design of the fluidized bed structure. Fig.6 shows the average temperature of solid particles in the fluidized bed solar particle receiver. It can be seen that after loading solar radiation, the particle temperature gradually increases. After 10 s, the particle temperature can reach 1645.34 K, the temperature rise exceeds 845 K, and the thermal efficiency is 50.53 %. However, with the passage of time, the rate of particle temperature rise gradually decreases, and the temperature of solid particles gradually tends to be stable.

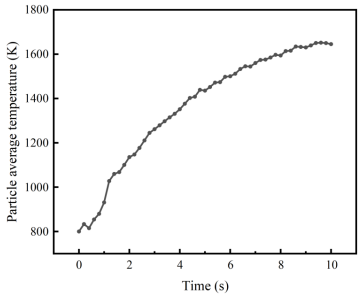

Figure 6: The average temperature of solid particles inside the receiver with time.

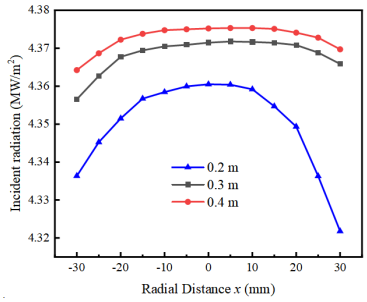

Figure 7: The radial radiation distribution of the central section at different heights

Fig.7 illustrates the radial radiation distribution of the central section at different heights. It can be seen that as the height increases, the radiation intensity gradually increases, and the radiation intensity at 0.2 m is significantly lower than which at the other two heights. This is because that the particles mainly move in the height range of 0-0.2m, and the radiation entering the receiver at the same position is absorbed by the solid particles, so that the radiation intensity at this height is lower. Besides, it is clear that the radiation intensity at both ends is lower than which at the center, which is similar to the Gaussian

ISSN 2706-655X Vol.6, Issue 4: 31-38, DOI: 10.25236/IJFET.2024.060406

distribution.

4. Conclusions

The gas-solid motion and heat transfer process of a three dimensional fluidized bed solar particle receiver is investigated by Euler-Euler model. The main results obtained from this study are concluded below:

(1) The solid particles show a clear symmetrical distribution in the receiver at the initial moment, which is a typical ring-core flow. The radial velocity distribution of particles at the bottom is opposite to the particles at top of the bed.

(2) The average temperature of the particles can reaching 1645.34 K after 10 s, but the temperature rise rate gradually weakens. The radiation intensity rises with the increase of axial height. In the radial direction, the distribution of radiation intensity shows a likely Gaussian distribution;

References

[1] Imran K M, Asfand F, Al-Ghamdi S G. Progress in technology advancements for next generation concentrated solar power using solid particle receivers[J]. Sustainable Energy Technologies and Assessments, 2022, 54: 102813.
[2] Stram B N. Key challenges to expanding renewable energy[J]. Energy Policy, 2016, 96: 728-734.
[3] Jiang K, Du X, Kong Y, et al. A comprehensive review on solid particle receivers of concentrated solar power[J]. Renewable and Sustainable Energy Reviews, 2019, 116: 109463.
[4] Benoit H, Spreafico L, Gauthier D, et al. Review of heat transfer fluids in tube-receivers used in concentrating solar thermal systems: Properties and heat transfer coefficients[J]. Renewable and Sustainable Energy Reviews, 2016, 55: 298-315.
[5] Falcone P K, Noring J E, Hruby J M. Assessment of a solid particle receiver for a high temperature solar central receiver system: SAND85-8208[R]. Sandia National Lab. (SNL-CA), Livermore, CA (United States), 1985.
[6] Hruby J M, Steele B R, Burolla V P. Solid particle receiver experiments: radiant heat test: SAND84-8251[R]. Sandia National Lab. (SNL-CA), Livermore, CA (United States), 1984.
[7] Rightley M J, Matthews L K, Mulholland G P. Experimental characterization of the heat transfer in a free-falling-particle receiver[J]. Solar Energy, 1992, 48(6): 363-374.
[8] Siegel N P, Ho C K, Khalsa S S, et al. Development and Evaluation of a Prototype Solid Particle Receiver: On-Sun Testing and Model Validation[J]. Journal of Solar Energy Engineering, 2010, 132(2).
[9] Ho C K, Christian J M, Romano D, et al. Characterization of Particle Flow in a Free-Falling Solar Particle Receiver[J]. Journal of Solar Energy Engineering, 2016, 139(2).
[10] Tan T, Chen Y. Review of study on solid particle solar receivers[J]. Renewable and Sustainable Energy Reviews, 2010, 14(1): 265-276.
[11] Sarker M R I, Mandal S, Tuly S S. Numerical study on the influence of vortex flow and recirculating flow into a solid particle solar receiver[J]. Renewable Energy, 2018, 129: 409-418.
[12] Sarker M R I, Saha M, Rahman M S, et al. Recirculating metallic particles for the efficiency enhancement of concentrated solar receivers[J]. Renewable Energy, 2016, 96: 850-862.
[13] Wu W, Amsbeck L, Buck R, et al. Proof of Concept Test of a Centrifugal Particle Receiver[J]. Energy Procedia, 2014, 49: 560-568.
[14] Wu W, Trebing D, Amsbeck L, et al. Prototype testing of a centrifugal particle receiver for high-temperature concentrating solar applications[J]. Journal of Solar Energy Engineering, Transactions of the ASME, 2015, 137(4).
[15] Wu W, Uhlig R, Buck R, et al. Numerical Simulation of a Centrifugal Particle Receiver for High-Temperature Concentrating Solar Applications[J]. Numerical Heat Transfer, Part A: Applications, 2015, 68(2): 133-149.
[16] Xiao G, Guo K, Luo Z, et al. Simulation and experimental study on a spiral solid particle solar receiver[J]. Applied Energy, 2014, 113: 178-188.
[17] Xiao G, Guo K, Ni M, et al. Optical and thermal performance of a high-temperature spiral solar particle receiver[J]. Solar Energy, 2014, Complete(109): 200-213.
[18] Patil A V, Peters E A J F, Kuipers J A M. Comparison of CFD–DEM heat transfer simulations with infrared/visual measurements[J]. Chemical Engineering Journal, 2015, 277: 388-401.